Heat Transfer Engineering, 25(2):30–40, 2004

ISSN: 0145-7632 print / 1521-0537 online
DOI: 10.1080/01457630490276097

Taylor & Francis
Taylor & Francis Group

Improved Heat Transfer Correlation in the Transition Region for a Circular Tube with Three Inlet Configurations Using Artificial Neural Networks

AFSHIN J. GHAJAR

School of Mechanical and Aerospace Engineering, Oklahoma State University, Stillwater, Oklahoma, USA

LAP MOU TAM

Department of Electromechanical Engineering, Faculty of Science and Technology, University of Macau, Taipa, Macau, China

SIK CHUNG TAM

Department of Mathematics, Faculty of Science and Technology, University of Macau, Taipa, Macau, China

Local forced and mixed heat transfer coefficients were measured by Ghajar and Tam [5] in a horizontal circular straight tube fitted with reentrant, square-edged, and bell-mouth inlets under uniform wall heat flux boundary condition. For the experiments, the Reynolds, Prandtl, and Grashof numbers varied from about 280 to 49000, 4 to 158, and 1000 to 2.5×10^5, respectively. The heat transfer transition regions were established by observing the change in the heat transfer behavior. The data in the transition region were correlated by using the traditional least squares method. The correlation predicted the transitional data with an average absolute deviation of about 8%. However, about 30% of the data in the transition region were predicted with 10–20% deviation, and about 3% with deviations greater than 20%. This is due to the abrupt change in the heat transfer characteristic and its intermittent behavior in this region. Since the value of the heat transfer coefficient has a direct impact on the size of the heat exchanger, a more accurate correlation has been developed using artificial neural networks. A total of 1290 data points (441 for reentrant, 416 for square-edged, and 433 for bell-mouth) were used. The accuracy of the improved heat transfer correlation is excellent, with the majority of the data points predicted with less than 5% deviation.

An important design problem in industrial heat exchangers arises when flow inside the tubes falls into the transition region. In practical engineering design, the usual recommendation is to avoid design and operation in this regime; however, this is not always feasible under design constraints. The usually cited transition Reynolds number of about 2100 applies, strictly speaking, to a very steady and uniform entry flow with a rounded entrance. If the flow has a disturbed entrance typical of heat exchangers, in which there is a sudden

Address correspondence to Dr. Afshin J. Ghajar, School of Mechanical and Aerospace Engineering, Oklahoma State University, Stillwater, Oklahoma 74078. E-mail: ghajar@ceat.okstate.edu

contraction and possibly even a reentrant entrance, the transition Reynolds number will be less. Experimental, numerical, and analytical studies are available for forced and mixed convection heat transfer in horizontal tubes with a rounded entrance in the laminar, transitional, and turbulent flow regimes. These works have been reviewed by Shah and London [1], Shah and Johnson [2], and Kakac and coworkers [3, 4]. However, very little information that is of immediate use to design engineers (i.e., correlation) is available to predict the developing and fully developed transitional forced and mixed convection heat transfer coefficients in a tube with a smooth or disturbed entrance. The correlation developed by Ghajar and Tam [5] is the only one that is available in the open literature for the above-mentioned case. Their correlation predicted the transitional data with an average absolute deviation of about 8%. However, about 30% of the data in the transition region were predicted with 10–20% deviation, and about 3% with deviations greater than 20%. Because the value of the heat transfer coefficient has a direct impact on the size of the heat exchanger, an accurate correlation is necessary. Because the traditional least squares method did not provide the desired accuracy for all the data points, an alternative method, the artificial neural networks (ANN), is employed. ANN has been successfully used in the analysis of heat transfer data and the heat transfer coefficient by Thibault and Grandjean [6] and Jambunathan et al. [7]. The applications of ANN in different areas in thermal engineering are well described in the comprehensive work done by Sen and Yang [8], Diaz et al. [9], Pacheco-Vega et al. [10, 11], and Diaz et al. [12]. In the work done in Pecheco-Vega et al. [10, 11], ANN and least squares methods were used to correlate the heat transfer coefficient and heat transfer rate directly. The results show that direct correlation for heat transfer rate is more accurate than the heat transfer coefficient. Direct prediction of heat transfer rate can help the user in evaluating the performance of heat exchanger easily; however, if the design of heat exchanger is the objective, the fundamental, which is the determination of heat transfer coefficient (i.e., the Nusselt number), is still absolutely necessary. The purpose of this study was to develop an accurate correlation using an unconventional method to correlate experimental data for a wide range of Reynolds, Prandtl, and Grashof numbers in the entrance and fully developed regions of a circular horizontal electrically heated straight tube fitted with three different inlet configurations (reentrant, square-edged, and bell-mouth).

HEAT TRANSFER EXPERIMENTS

The heat transfer experimental data used in this study, along with a detailed description of the experimental apparatus and procedures used, were reported by Ghajar and Tam [5]. A schematic of the overall experimental setup used for heat transfer measurements is shown in Figure 1. In this paper, only a brief description of the experimental setup and procedures will be provided. The

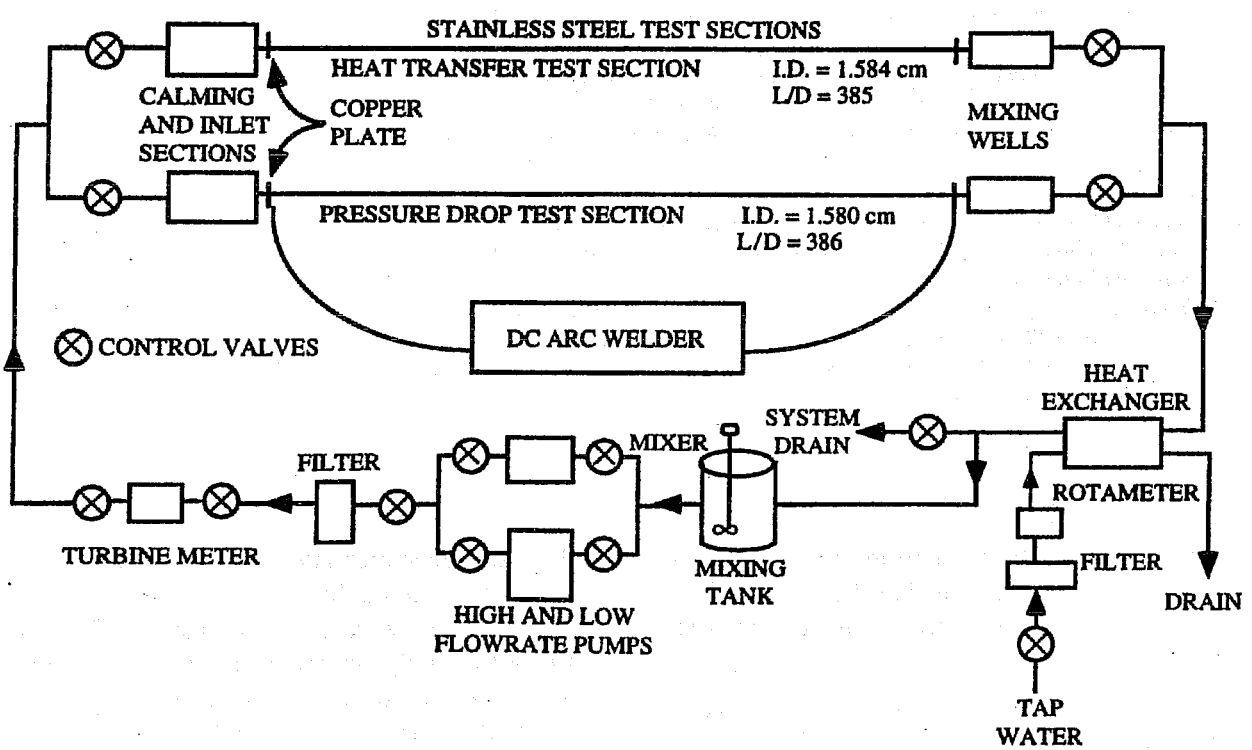

Figure 1 Schematic diagram of experimental setup.

local forced and mixed convective measurements were made in a horizontal, electrically heated, stainless steel circular straight tube with reentrant, square-edged, and bell-mouth inlets under a uniform wall heat flux condition. The pipe had an inside diameter of 1.58 cm and an outside diameter of 1.90 cm. The total length of the test section was 6.10 m, providing a maximum length-to-inside diameter ratio of 385. A uniform wall heat flux boundary condition was maintained by a dc arc welder. Thermocouples (T-type) were placed on the outer surface of the tube wall at close intervals near the entrance and at greater intervals further downstream. Twenty-six axial locations were designated, with four thermocouples placed at each location. The thermocouples were placed 90° apart around the periphery. From the local peripheral wall temperature measurements at each axial location, the inside wall temperatures and the local heat transfer coefficients were calculated. In these calculations, the axial conduction was assumed negligible (RePr > 4,200 in all cases), but peripheral and radial conduction of heat in the tube wall were included. In addition, the bulk fluid temperature was assumed to increase linearly from the inlet to the outlet. As reported by Ghajar and Tam [5], the uncertainty analyses of the overall experimental procedures showed that there is a maximum of 9% uncertainty for the heat transfer coefficient calculations. Moreover, the heat balance error for each experimental run indicates that in general, the heat balance error is less than 5%. For Reynolds numbers lower than 2500 where the flow is strongly influenced by secondary flow, the heat balance error is slightly higher (5–8%) for that particular Reynolds number range.

To ensure a uniform velocity distribution in the test fluid before it entered the test section, the flow passed through calming and inlet sections. The calming section had a total length of 61.6 cm and consisted of a 17.8 cm-diameter acrylic cylinder with three perforated acrylic plates, followed by tightly packed soda straws sandwiched between galvanized steel mesh screens. Before entering the inlet section, the test fluid passed through a fine mesh screen and flowed undisturbed through 23.5 cm of a 6.5 cm-diameter acrylic tube before it entered the test section. The inlet section had the versatility of being modified to incorporate a reentrant or bell mouth inlet (see Figure 2). The reentrant inlet was simulated by sliding 1.93 cm of the tube entrance length into the inlet section, which was otherwise the square-edged (sudden contraction) inlet. For the bell-mouth inlet, a fiberglass nozzle with a contraction ratio of 10.7 and a total length of 23.5 cm was used in place of the inlet section.

In the experiments, distilled water and mixtures of distilled water and ethylene glycol were used. The

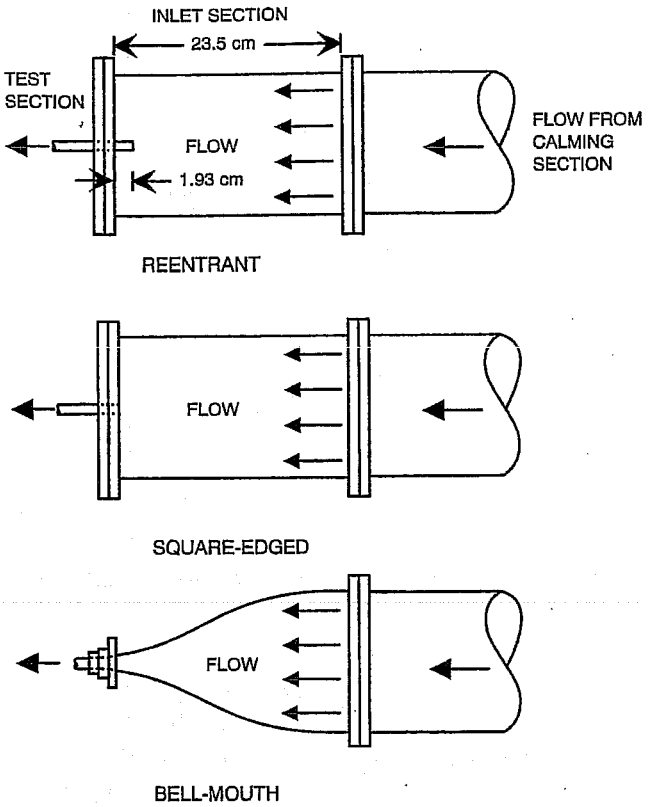

Figure 2 Schematic of the three different inlet configurations.

experiments covered the local bulk Reynolds number range of 280 to 49000, the local Prandtl number range of 4 to 158, the local bulk Grashof number range of 1000 to 2.5×10^5, and the local bulk Nusselt number range of 13 to 258. The wall heat flux for the experiments ranged from 4 to 670 kW/m^2.

CORRELATION USING ARTIFICIAL NEURAL NETWORKS

Figure 3 shows the heat transfer data for the transition region for the reentrant, square-edged, and bell-mouth inlet configurations. The figure clearly shows the influence of inlet configuration on the beginning and end of the heat transfer transition region. Figure 3 plots the local average peripheral heat transfer coefficients in terms of the Colburn j factor ($StPr^{0.6}$) versus local bulk Reynolds number for all flow regimes at the length-to-inside diameter ratio of 192. The filled symbols represent the start and end of the heat transfer transition region for each inlet configuration.

Figure 3, for comparison purposes, also shows the typical fully developed pipe flow forced convection heat transfer correlations for turbulent [13] and laminar ($Nu = 4.364$) flows under the uniform wall heat flux boundary condition. In the turbulent flow regime, for Reynolds numbers greater than about 8500 to 10,500

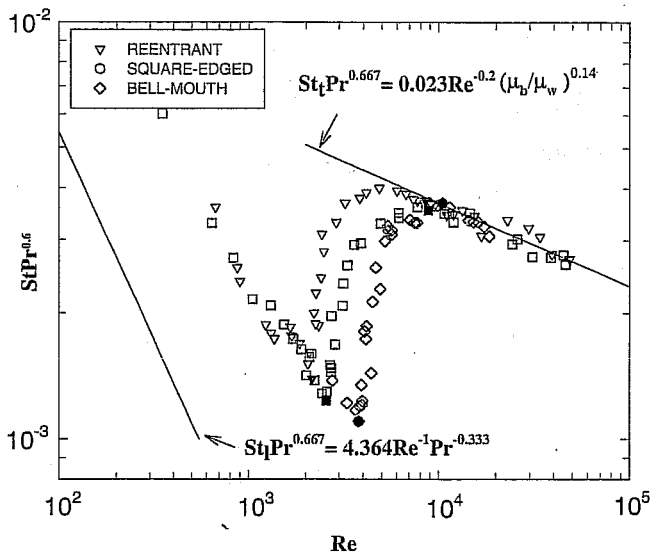

Figure 3 Heat transfer in the transition region (solid symbols designate the start and end of the transition region for each inlet).

(depending on the inlet type), the experimental data appear on the turbulent heat transfer line (within ±8%). However, in the laminar flow regime, for Reynolds numbers less than about 2000 to 3800 (depending on the inlet type), the data appear to have a pronounced and almost parallel shift above the accepted laminar heat transfer line. This is directly due to the strong influence of buoyancy forces (free convection) on forced convection, giving rise to mixed convection heat transfer. This in turn results in a higher fully developed laminar uniform wall heat flux Nusselt number than the accepted 4.364 value (a value of about 14.5 is estimated for the data). It should be noted that in the fully developed laminar flow region, no forced convection data could be obtained. At the minimum welder current setting (approximately 150 A), the heat generated at the tube wall was enough to bring about peripheral temperature variations extensive enough to cause secondary flow.

As seen in Figure 3, the abrupt change of heat transfer characteristic in the transition region is obvious. In this region, the flow has both laminar and turbulent characteristics. In addition, the type of inlet configuration influences the beginning and end of the transition region. Ghajar and Tam [5] used the asymptotic method similar to Churchill [14] to develop a correlation in the transition region since the variation of heat transfer coefficient, as indicated by Figure 3, is between two asymptotes. The correlation is

$$\mathrm{Nu}_{tr} = \mathrm{Nu}_l + \left\{\exp[(a - \mathrm{Re})/b] + \mathrm{Nu}_t^c\right\}^c \qquad (1)$$

where Nu_l (laminar flow Nusselt number) is given in Eq. (2), Nu_t (turbulent flow Nusselt number) is given in Eq. (3), and the values of the suggested constants a, b, and c for each inlet are summarized in Table 1:

Table 1 Constants for Eq. (1)

Inlet	a	b	c
Reentrant	1766	276	−0.955
Square-edged	2617	207	−0.950
Bell-mouth	6628	237	−0.980

$$\mathrm{Nu}_l = 1.24[(\mathrm{RePr}D/x) + 0.025(\mathrm{GrPr})^{0.8}]^{0.33}(\mu_b/\mu_w)^{0.14} \qquad (2)$$

$$\mathrm{Nu}_t = 0.023\mathrm{Re}^{0.8}\mathrm{Pr}^{0.385}(x/D)^{-0.0054}(\mu_b/\mu_w)^{0.14} \qquad (3)$$

The range of independent variables used in Eq. (1) is as follows:

Reentrant: $3 \le x/D \le 192$, $1700 \le \mathrm{Re} \le 9100$, $5 \le \mathrm{Pr} \le 51$, $4000 \le \mathrm{Gr} \le 2.1 \times 10^5$, and $1.2 \le \mu_b/\mu_w \le 2.2$

Square-edged: $3 \le x/D \le 192$, $1600 \le \mathrm{Re} \le 10{,}700$, $5 \le \mathrm{Pr} \le 55$, $4000 \le \mathrm{Gr} \le 2.5 \times 10^5$, and $1.2 \le \mu_b/\mu_w \le 2.6$

Bell-mouth: $3 \le x/D \le 192$, $3300 \le \mathrm{Re} \le 11{,}100$, $13 \le \mathrm{Pr} \le 77$, $6000 \le \mathrm{Gr} \le 1.1 \times 10^5$, and $1.2 \le \mu_b/\mu_w \le 3.1$

Eq. (1) is applicable to transition forced and mixed convection in the entrance and fully developed regions and should be used with an appropriate set of constants for each inlet configuration. Figure 4 compares the predicted Nusselt numbers obtained from Eq. (1) for each inlet configuration with measurements. Table 2 summarizes the percent deviations between the experimental data and the predictions of Eq. (1) for the three inlet configurations.

As seen in Table 2, there is still plenty of room for improving the accuracy of the correlation. Because the accuracy of the heat transfer coefficient has a direct impact on the size of the heat exchanger, a correlation with high accuracy using artificial neural networks (ANN) is introduced.

The ANN employed in this paper is called a three-layer feedforward neural network. This type of network has become very popular in engineering applications. Its typical graphical representation is shown in Figure 5. As shown in this figure the ANN consists of three layers, namely, the input layer the hidden layer, and the output layer. The input layer, receives R independent inputs p_1, $p_2, \ldots, p_R$ to the ANN and passes them to the hidden layer. In the hidden layer, each neuron first calculates the correspondent weighted sum of $p_1, p_2, \ldots, p_R$ from the

Table 2 Percent deviations between the experimental data and predictions of Eq. (1)

	Reentrant	Square-edged	Bell-mouth
Total data used	441 data points	416 data points	433 data points
Dev. range	−23 to +25.1%	−23.9 to +24.3%	−22 to +18.5%
> 20% dev.	3% (13 pts)	3% (12 pts)	1% (4 pts)
10 to 20% dev.	29% (129 pts)	26% (106 pts)	24% (104 pts)
<10% dev.	68% (299 pts)	72% (298 pts)	75% (325 pts)
Avg. abs. dev.	8%	7.2%	8.1%

input layer and its bias. Hence, for $j = 1, 2, \ldots, S$, the jth neuron will give the sum $\sum_{k=1}^{R} w_{jk}^{1} p_k + b_j^1$, which is called the net input of the jth neuron of the hidden layer. Secondly, the neuron applies a function f, the transfer function, to its net inputs, and passes the resulting value to the output layer. Therefore, the jth neuron will produce $f(\sum_{k=1}^{R} w_{jk}^{1} p_k + b_j^1)$, the output of the hidden layer. In this study, the transfer function of the hidden layer is a sigmoid function $f(s) = [1 - \exp(s)]^{-1}$. Eventually, the unique neuron in the output layer sums all the correspondent weighted outputs of the hidden layer and its bias, b_1^2, and transforms this sum linearly (the transfer function is defined to be $y = x$ in this layer) to produce a number, the network output a, which is therefore equal to $\sum_{j=1}^{S} w_{1j}^{2} f(\sum_{k=1}^{R} w_{jk}^{1} p_k + b_j^1) + b_1^2$. In Hornik [15], it is shown that the above ANN is a universal approximator. Hence, it is practically able to model almost any nonlinear correlation with R variables. To apply the ANN method, the number of the neurons of the hidden layer S has to be chosen and fixed first in order to determine the structure of the ANN. Secondly, other parameters such as the weights and biases, are identified by minimizing the square sums of the difference between the output of the ANN and the corresponding experimental reading. Usually, a gradient-based method will be employed for such optimizations. In this case, the related gradients should be found numerically and is confirmed by backpropagation algorithm. The backpropagation algorithm proposed by Rumelhart et al. [16] is the core result of the supervised learning theory of ANN. Mathematically, it provides us with a unified and efficient way to calculate all the corresponding gradients with any choice of fixed value S. The selection of the gradient-based method depends on the data set as well as the application itself. The steepest descent

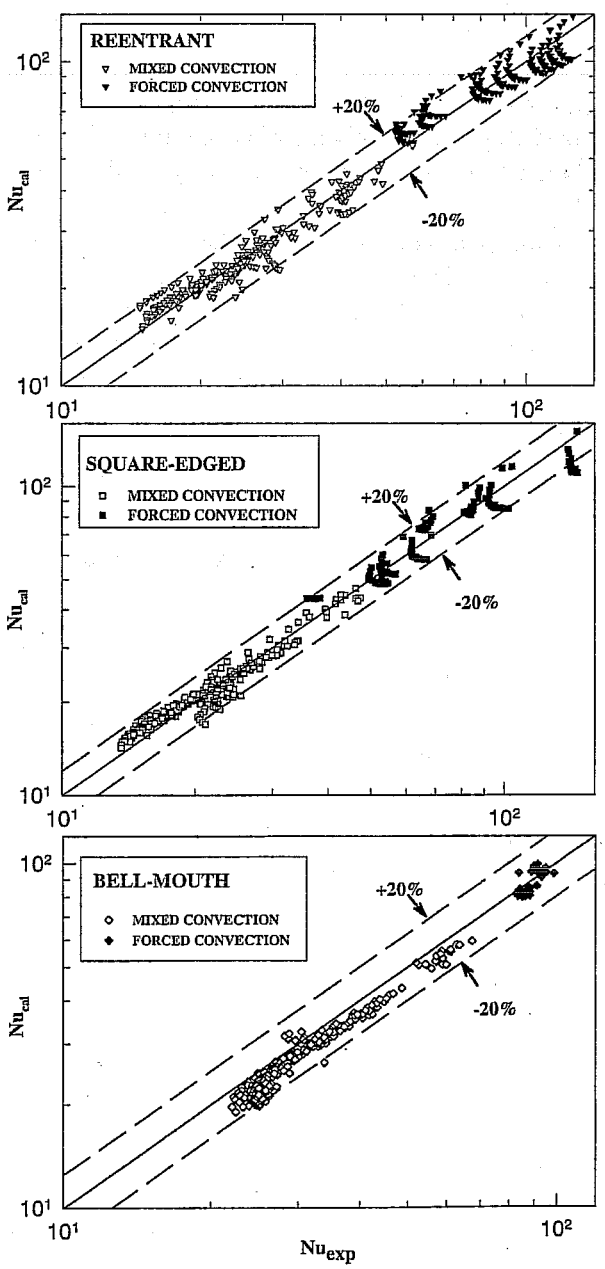

Figure 4 Comparisons between experimental Nusselt numbers and predicted Nusselt numbers using Eq. (1).

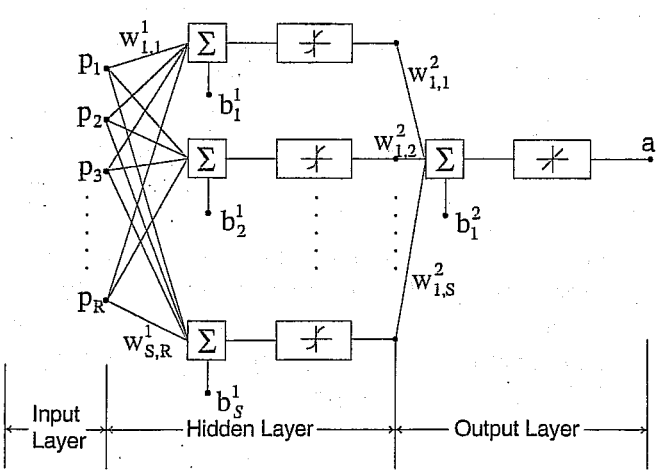

Figure 5 A three-layer network with S neurons in its hidden layer.

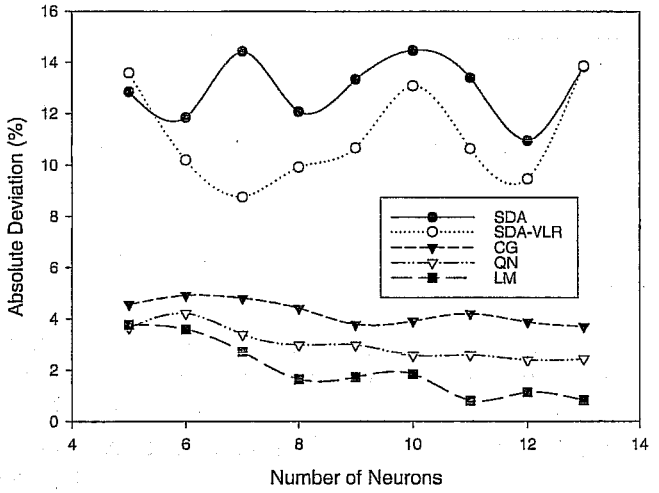

Figure 6 Determination of the backpropagation method and the number of neurons used in the hidden layer.

algorithm is the general choice. For fast convergence, more recent algorithms used heuristic techniques, such as those by Jacobs [17] and Vogl et al. [18], and standard numerical optimization techniques like the work done by Barnard [19], Batti [20], and Charalambous [21] are also available for consideration.

In this study, the reentrant data (441 points) is used to determine the type of backpropagation method and the number of neurons used in the hidden layer. The methods to be compared are Steepest Descent Algorithm (SDA), Steepest Descent Algorithm with Variable Learning Rate (SDA-VLR), Conjugate Gradient (CG), Quasi-Newton (QN), and the Levenberg-Marquardt (LM). The reentrant data was pretrained and precorrelated using different methods and neuron combinations. The absolute deviation for the data is used as the method–neuron chosen criteria. The maximum number of iterations was set as 10,000, and all of the initial random weights and biases were fixed for each gradient method. MATLAB (R.12.1) is used to implement the three-layer feedforward neural network.

As seen in Figure 6, when the method is selected as LM and the number of neurons equals 11, the absolute deviation is the smallest amongst all the methods. Therefore, the backpropagation used in this study is the Levenberg-Marquardt (LM) method and the number of neurons used in this study is set to 11. Moreover, the learning rate of the LM method is 0.0001. When the epoch reaches 1000, the training stops. After the backpropagation has been completed and the postprocessing of the network output has been performed, the resulted neural network, which is the proposed improved correlation, is given in a simple matrix form. The proposed improved heat transfer correlation is:

$$\mathrm{Nu} = u^3\{(u^2)^2 f(u^1\Phi + v^1) + v^2\} + v^3 \qquad (4)$$

where

$$f(s) = [1 - \exp(s)]^{-1}$$

$$\Phi = \begin{bmatrix} \mathrm{Re}_{\mathrm{normal}} \\ \mathrm{Pr}_{\mathrm{normal}} \\ \mathrm{Gr}_{\mathrm{normal}} \\ X/D_{\mathrm{normal}} \\ \left(\frac{\mu_b}{\mu_w}\right)^{0.14}_{\mathrm{normal}} \end{bmatrix}$$

$$= \begin{bmatrix} 2(\mathrm{Re} - \mathrm{Re}_{\min})/(\mathrm{Re}_{\max} - \mathrm{Re}_{\min}) - 1 \\ 2(\mathrm{Pr} - \mathrm{Pr}_{\min})/(\mathrm{Pr}_{\max} - \mathrm{Pr}_{\min}) - 1 \\ 2(\mathrm{Gr} - \mathrm{Gr}_{\min})/(\mathrm{Gr}_{\max} - \mathrm{Gr}_{\min}) - 1 \\ 2(x/D - x/D_{\min})/(x/D_{\max} - x/D_{\min}) - 1 \\ 2\left(\left(\frac{\mu_b}{\mu_w}\right)^{0.14} - \left(\frac{\mu_b}{\mu_w}\right)^{0.14}_{\min}\right)\Big/\left(\left(\frac{\mu_b}{\mu_w}\right)^{0.14}_{\max} - \left(\frac{\mu_b}{\mu_w}\right)^{0.14}_{\min}\right) - 1 \end{bmatrix}$$

The entries of the vector Φ represent the normalized Reynolds number, Prandtl number, Grashof number, x/D, and μ ratio, respectively. In this study, only 80% of the experimental data for each inlet were used to establish the correlation's constant matrices as indicated in Eq. (4). The rest of the data (i.e., 20%) were used for the network testing. The numerical values for the matrices and scalars for different inlet configurations are as follow.

For the reentrant inlet configuration,

$$u^1 = \begin{bmatrix} 0.94 & 1.78 & 3.43 & 11.21 & -1.18 \\ 0.42 & -0.01 & 1.39 & -0.03 & 1.62 \\ -7.83 & 14.17 & -5.10 & -0.04 & -0.06 \\ -2.05 & 2.50 & 1.51 & 0.30 & -1.62 \\ -2.90 & -3.60 & 3.07 & -0.10 & -2.73 \\ 2.33 & 1.89 & -0.40 & -0.40 & 1.31 \\ -1.09 & 0.63 & -2.39 & 0.03 & -0.38 \\ -5.89 & -26.99 & -28.11 & 1.84 & -4.98 \\ -0.79 & 0.20 & -2.66 & 0.01 & 0.07 \\ 0.81 & 0.72 & 1.81 & 9.29 & -0.80 \\ -33.66 & 15.59 & 47.16 & 1.00 & -2.20 \end{bmatrix},$$

$$u^2 = \begin{bmatrix} 1.20 \\ -9.80 \\ 0.94 \\ 21.41 \\ -2.84 \\ 16.75 \\ -44.09 \\ 0.28 \\ 72.90 \\ -1.80 \\ -0.47 \end{bmatrix}, \quad u^3 = 55.76,$$

$$v^1 = \begin{bmatrix} 13.52 \\ 2.74 \\ -4.54 \\ -0.30 \\ 0.38 \\ 0.85 \\ -3.50 \\ -4.16 \\ -4.43 \\ 13.73 \\ 1.09 \end{bmatrix}, \quad v^2 = 10.01, \quad v^3 = 14.74$$

For the square-edged inlet configuration,

$$u^1 = \begin{bmatrix} 0.70 & -1.17 & -26.19 & -6.88 & 4.06 \\ 1.59 & -1.98 & -1.42 & -0.07 & -3.79 \\ -10.53 & 9.63 & 3.71 & 0.43 & -4.41 \\ -0.40 & 1.07 & 21.39 & 6.56 & -3.33 \\ 41.81 & 1.90 & -15.81 & 2.49 & 1.17 \\ -0.37 & -1.18 & 25.86 & -2.23 & 1.11 \\ -16.18 & 12.31 & -8.20 & 0.10 & -4.25 \\ -8.19 & -3.31 & 3.29 & 2.69 & -1.30 \\ 0.87 & -2.03 & -1.04 & -0.19 & -2.49 \\ -1.63 & 0.14 & -0.69 & -0.58 & 4.40 \\ -0.83 & 1.68 & 0.98 & 0.08 & 2.61 \end{bmatrix},$$

$$u^2 = \begin{bmatrix} -12.03 \\ 20.36 \\ 3.66 \\ -40.65 \\ 0.37 \\ 0.13 \\ -0.18 \\ -0.19 \\ 14.87 \\ -1.63 \\ 33.98 \end{bmatrix}, \quad u^3 = 66.44,$$

$$v^1 = \begin{bmatrix} -29.45 \\ -4.93 \\ 6.98 \\ 26.55 \\ 12.52 \\ 27.07 \\ -6.65 \\ 0.83 \\ -2.00 \\ 1.30 \\ 2.88 \end{bmatrix}, \quad v^2 = 4.95, \quad v^3 = 13.54$$

For the bell-mouth inlet configuration,

$$u^1 = \begin{bmatrix} -0.45 & -7.28 & -3.50 & -0.60 & -6.31 \\ -11.26 & -40.91 & -24.10 & 1.18 & 7.65 \\ -0.66 & -3.13 & -1.12 & 0.94 & 0.51 \\ 2.06 & 6.08 & 3.24 & 3.26 & 1.28 \\ 8.42 & -6.94 & 7.09 & -2.221 & -6.35 \\ 3.29 & -6.77 & 6.76 & -1.12 & -5.01 \\ 1.39 & -1.51 & 1.36 & -0.02 & -0.42 \\ -3.60 & -1.68 & 3.92 & -34.85 & -23.67 \\ 3.88 & 1.86 & -3.04 & -0.53 & -2.41 \\ 1.03 & -1.96 & 0.90 & 0.08 & -0.26 \\ -1.49 & -0.34 & -0.29 & -14.33 & 1.88 \end{bmatrix},$$

$$u^2 = \begin{bmatrix} 1.26 \\ 0.10 \\ 1.34 \\ -0.16 \\ 0.61 \\ 0.27 \\ 12.14 \\ -0.02 \\ 0.96 \\ -13.42 \\ 19.24 \end{bmatrix}, \quad u^3 = 46.81,$$

$$v^1 = \begin{bmatrix} -8.43 \\ -19.00 \\ -1.70 \\ 4.99 \\ 0.25 \\ 3.82 \\ 2.25 \\ -24.87 \\ -3.66 \\ 1.58 \\ -19.28 \end{bmatrix}, \quad v^2 = -0.06, \quad v^3 = 22.1$$

Tables 3–5 summarize the accuracy of the proposed ANN heat transfer correlation for the three different inlet configurations. Note that for comparison purposes, the tables show the accuracy distribution for 100% of the experimental data (denoted by M), the data that were used to train the network (denoted by M_a i.e., 80% of M), and the data that were never used in training but were used for testing (denoted by M_b). Figure 7 compares the predicted Nusselt numbers obtained from the proposed ANN-based correlation for each inlet configuration with measurements.

The proposed ANN correlation is applicable to the developing and fully developed transition regions. As

Table 3 Accuracy of the proposed reentrant correlation

	Reentrant Inlet, $M = 441$ pts, $M_a = 353$ pts, $M_b = 88$ pts				
	Range of deviation	Absolute deviation	Less than ±5% deviation	Between ±5% and 10% deviation	More than ±10% deviation
M	−11.35% to 7.49%	1.12%	428 data points	12 data points	1 data point
M_a	−8.82% to 7.49%	1.00%	347 data points	6 data points	0 data points
M_b	−11.35% to 6.75%	1.60%	81 data points	6 data points	1 data point

seen in Tables 3–5 and Figure 7, all of the experimental data for the bell-mouth inlet are predicted with less than 5% deviation. For the square-edged inlet, 99.5 percent of the data are predicted with less than 5% deviation; only two data points, one from the training set and the other from the testing set, are predicted with a little more than 5% deviation. For the reentrant inlet, practically all of the data are predicted with less than 5% deviation (97.1%). Only twelve data points, six from the training set and six from the testing set, are predicted with 5–10% deviation, and only one data point is predicted with more than 10% deviation (11.35%). Compared to the accuracy provided by the traditional method, it can be concluded that the ANN correlation outperforms the traditional least squares method correlation.

It is worthy to have a discussion to compare the ANN method with the traditional least squares regression method. In Ghajar and Tam [5], the form of the equation for the least squares regression was determined before the regression. Determination of the form may be difficult and is time-consuming. Usually, the form of the correlation is either empirical or semi-empirical, and therefore a lot of unknown factors may influence the accuracy of the correlation. On the other hand, the proposed one hidden layer network, as seen in the theorem of Hornik [15], has the ability to approximate the unknown nonlinear target correlation by simply choosing an appropriate number of neurons in the hidden layer. By examining the internal structure of the networks, it can be observed that the number of weights and biases will increase or decrease linearly with the input dimension if we add or remove (respectively) a neuron from the hidden layer. In finding a network for better precision, the complexity of the structure of the network would not be influenced significantly by changing the number of hidden neurons due to the linear growth of the parameters. However, for the least squares regression, improving precision may involve (1) the determination of a better functional form, empirically or semi-empirically, and/or (2) the addition of extra variables through some difficult experimental processes. For example, in this case, it is necessary to either change the form of Eq. (1) or add one or more independent variables besides Re, Pr, Gr, $(\mu_b/\mu_w)^{0.14}$, and x/D. Neither is an easy nor obvious task. Moreover, nontrivial and complicated computation may need to be performed in order to obtain the gradient of the new correlation form for least squares optimization. In this study, we benefited from the backpropagation algorithm, a general way to compute the gradient of the kind of networks easily with various numbers of hidden neurons. Therefore—again, according to the linear growth of the parameters and the backpropagation algorithm—the computation complexity is still well under control. Furthermore, unlike the traditional methods, inexpensive parallel computing using a Linux PC cluster can be used in the simulation and the training of ANN to reduce the computational time in training a huge amount of experimental data. One of the drawbacks regarding the ANN method is the "black box" characteristic—the correlation form could not quantify the contributions from independent inputs. For example, besides the normalized Re, Pr, Gr, X/D, and μ_b/μ_w, if an additional input parameter is added, it is hard to tell whether this input parameter is redundant. One of the methods that can quantify the contributions from various inputs is the use of genetic algorithm (GA). The use of GA can find the fewest number of input variables (or near the optimal number) [22–25]. Even with reduced inputs, the network performance, according to the literature, is still comparable with the

Table 4 Accuracy of the proposed square-edged correlation

	Square-edged Inlet, $M = 416$ pts, $M_a = 333$ pts, $M_b = 83$ pts			
	Range of deviation	Absolute deviation	Less than ±5% deviation	Between ±5% and ±10% deviation
M	−4.88% to 5.24%	1.06%	414 data points	2 data points
M_a	−4.24% to 5.16%	1.03%	332 data points	1 data point
M_b	−4.88% to 5.24%	1.16%	82 data points	1 data point

Table 5 Accuracy of the proposed bell-mouth correlation

	Bell-mouth Inlet, $M = 433$ pts, $M_a = 347$ pts, $M_b = 87$ pts		
	Range of deviation	Absolute deviation	Less than ±5% deviation
M	−3.45% to 3.60%	0.62%	433 data points
M_a	−2.56% to 2.29%	0.59%	347 data points
M_b	−3.45% to 3.60%	0.74%	87 data points

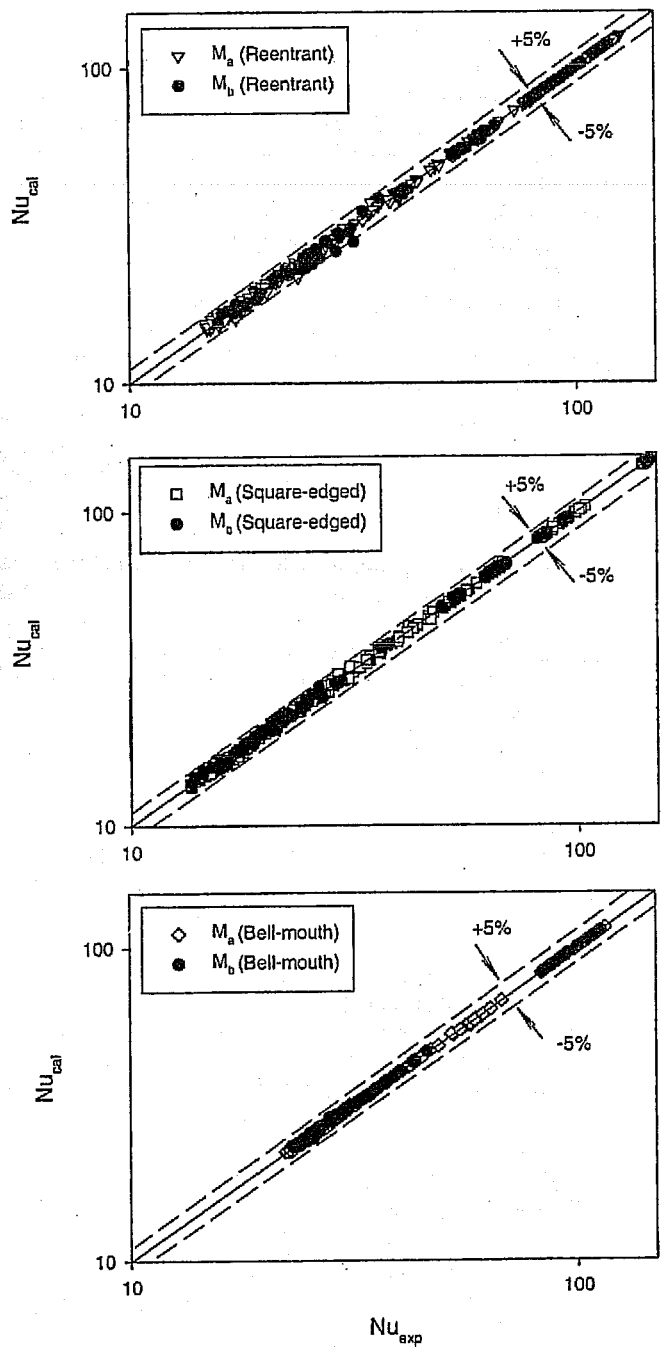

Figure 7 Comparisons between experimental Nusselt numbers and those predicted by the proposed ANN-based transition region heat transfer correlation.

original network because of all of the input variables. The GA's implementation for the input variables selection is shown in [26]. In, a pre-preprocessing step, the total number of input variables is set equal to the length of a binary chromosome. Each bit corresponds to an input: "1" indicates the presence of an input variable, and "0" indicates the absence of the input variable. Training an ANN with these inputs and using the performance error of the ANN to calculate its fitness value carry out the evaluation of an individual chromosome. According to the fitness value, which is used to evaluate the usefulness of the chromosomes, the best binary string can be achieved and the least significant variable(s) may drop out based on this binary string. Even though this method was originally proposed to be used in image recognition and classification problems, it is believed that the above-mentioned method can be used to identify the importance of the input variables.

This study provided an improved correlation for heat transfer in the transition region for the three different inlet configurations using an alternative method, the artificial neural networks. The heat transfer correlation developed in this study can be used to assist the heat exchanger designer in predicting the heat transfer coefficient along a horizontal straight circular tube with uniform wall heat flux for a specified inlet configuration in the transition region.

NOMENCLATURE

a	constant in Eq. (1) or scalar ANN output (see Figure 5)
b	constant in Eq. (1) or bias
c	constant in Eq. (1)
c_p	specific heat of the test fluid at the bulk temperature
D	inside diameter of tube
f	transfer function
g	acceleration of gravity
Gr	local bulk Grashof number, $g\beta\rho^2 D^3(T_w - T_b)/\mu^2$
h	local average or fully developed peripheral heat transfer coefficient
k	thermal conductivity of the test fluid at the bulk temperature
M	total number of experimental data points
M_a	number of experimental data points used for training
M_b	number of experimental data points used for testing
Nu	local Nusselt number, hD/k
p	scalar input
Pr	local bulk Prandtl number, $\mu c_p/k$
R	total number of network inputs (independent variables)
Re	local bulk Reynolds number, $\rho VD/\mu$

S total number of neurons in a hidden layer
T temperature
u constant matrix
v constant matrix
V average velocity in the test section
w scalar weight
x local distance

Greek

β coefficient of thermal expansion of the test fluid at the bulk temperature
ρ density of the test fluid at the bulk temperature
μ dynamic viscosity
Φ normalized input vector

Subscripts

b bulk
l laminar
t turbulent
tr transition
w wall

REFERENCES

[1] Shah, R. K., and London, A. L., *Laminar Flow Forced Convection in Ducts, a Supplement to Advances in Heat Transfer*, Academic, New York, 1978.

[2] Shah, R. K., and Johnson, R. S., Correlations for Fully Developed Turbulent Flow Through Circular and Noncircular Channels, *Sixth National Heat and Mass Transfer Conf.*, Indian Institute of Technology, Madras, India, pp. D75–D95, 1981.

[3] Kakac, S., Shah, R. K., and Bergles, A. E., *Low Reynolds Number Flow Heat Exchanger*, Hemisphere, New York, 1981.

[4] Kakac, S., Shah, R. K., and Aung, W., *Handbook of Single-Phase Convective Heat Transfer*, Wiley, New York, 1987.

[5] Ghajar, A. J., and Tam, L. M., Heat Transfer Measurements and Correlations in the Transition Region for a Circular Tube with Three Different Inlet Configurations, *Experimental Thermal and Fluid Science*, vol. 8, no. 1, pp. 79–90, 1994.

[6] Thibault, J., and Grandjean, B. P. A., A Neural Network Methodology for Heat Transfer Data Analysis, *Int. J. Heat Mass Transfer*, vol. 34, no. 8, pp. 2063–2070, 1991.

[7] Jambunathan, K., Hartle, S. L., Ashforth-Frost, S., and Fontama, V. N., Evaluating Convective Heat Transfer Coefficients Using Neural Networks, *Int. J. Heat Mass Transfer.*, vol. 39, no. 11, pp. 2329–2332, 1996.

[8] Sen, M., and Yang, K. T., Applications of Artificial Neural Networks and Genetic Algorithms in Thermal Engineering, *CRC Handbook of Thermal Engineering*, ed., F. Kreith, Section 4.24, Boca Raton, FL, pp. 620–661, 1999.

[9] Diaz, G., Sen, M., Yang, K. T., McClain, R. L., Simulation of Heat Exchanger Performance by Artificial Neural Networks, *HVAC&R Research*, vol. 5, no. 3, pp. 195–208, 1999.

[10] Pacheco-Vega, A., Sen, M., Yang, K. T., and McClain, R. L., Neural Network Analysis of Fin-Tube Refrigerating Heat Exchanger with Limited Experimental Data, *Int. J. of Heat and Mass Transfer*, vol. 44, pp. 763–770, 2001.

[11] Pacheco-Vega, A., Diaz, G., Sen, M., Yang, K. T., and McClain, R. L., Heat Rate Predictions in Humid Air-Water Heat Exchangers Using Correlations and Neural Networks, *ASME Trans.*, vol. 123, pp. 348–354, 2001.

[12] Diaz, G., Sen, M., Yang, K. T., McClain, R. L., Adaptive Neurocontrol of Heat Exchanger, *ASME Trans.*, vol. 123, pp. 556–562, 2001.

[13] Sieder, E. N., and Tate, G. E., Heat Transfer and Pressure Drop in Liquids in Tubes, *Ind. Eng. Chem.*, vol. 28, pp. 1429–1435, 1936.

[14] Churchill, S. W., Comprehensive Correlating Equations for Heat, Mass, and Momentum Transfer in Fully Developed Flow in Smooth Tubes, *Ind. Eng. Chem. Fundam.*, vol. 16, no. 1, pp. 109–116, 1977.

[15] Hornik, K., Approximation Capabilities of Multilayer Feedforward Networks, *Neural Networks*, vol. 4, no. 2, pp. 251–257, 1991.

[16] Rumelhart, D. E., Hinton, G. E., and Williams, R. J., Learning Internal Representations by Error Propagation, *Parallel Distributed Processing: Explorations in the Microstructure of Cognition*, vol. 1, eds. D. E. Rumelhart and J. L. McClelland, pp. 318–362, MIT Press, Cambridge, Mass., 1986.

[17] Jacobs, R. A., Increased Rates of Convergence through Learning Rate Adaptation, *Neural Networks*, vol. 1, no. 4, pp. 295–308, 1988.

[18] Vogl, T. P., Mangis, J. K., Zigler, A. K., Zink, W. T., and Alkon, D. L., Accelerating the Convergence of the Backpropagation Method, *Biological Cybernetics*, vol. 59, pp. 256–264, 1988.

[19] Barnard, E., Optimization for Training Neural Nets, *IEEE Transactions on Neural Networks*, vol. 3, no. 2, pp. 232–240, 1992.

[20] Batti, R., First and Second Order Methods for Learning: Between Steepest Descent and Newton's Method, *Neural Computation*, vol. 4, no. 2, pp. 141–166, 1992.

[21] Charalambous, C., Conjugate Gradient Algorithm for Efficient Training of Artificial Neural Networks, Circuits, Devices and Systems, *IEEE Proceedings*, vol. 139, no. 3, pp. 301–310, June 1992.

[22] D'Heygere, T., Goethals, P. L. M., and Pauw, N. De, Use of Genetic Algorithms to Select Input Variables in Artificial Neural Network Models for the Prediction of Benthic Macroinvertebrates, *Proceedings of the First Biennial Meeting of the International Environmental Modelling and Software Society*, vol. 2, pp. 136–141, June 2002.

[23] Jack, L. B., and Nandi, A. K., Feature Selection for ANNs Using Genetic Algorithms in Condition Monitoring, *ESANN 1999 Proceedings of the 7th European Symposium on Artificial Neural Networks*, Bruges, Belgium, pp. 313–318, April 1999.

[24] Cantú-Paz, E., and Kamath, C., Evolving Neural Networks to Identify Bent-double Galaxies in the FIRST Survey, *Neural Networks*, vol. 16, pp. 507–517, 2003.

[25] Guo, Z., and Uhrig, R. E., Using Genetic Algorithms to Select Inputs for Neural Networks, *Proceedings of COGANN-92*, eds., D. Whitley and J.D. Schaffer, IEEE, Computer Society Press, Baltimore, MD, pp. 223–234, June 1992.

[26] Yao, X., Evolving Artificial Neural Networks, *Proceedings of the IEEE*, vol. 87, no. 9, pp. 1423–1447, Sep 1999.

Afshin J. Ghajar is a Regents Professor and Director of Graduate Studies in the School of Mechanical and Aerospace Engineering at Oklahoma State University. He received his BS, MS, and Ph.D. all in Mechanical Engineering from Oklahoma State University. His expertise is in experimental and computational heat transfer and fluid mechanics. Dr. Ghajar has been a Summer Research Fellow at Wright Patterson AFB (Dayton, Ohio) and Dow Chemical Company (Freeport, Texas). He and his coworkers have published over 100 reviewed research papers. He has received several outstanding teaching awards: The Regents Distinguished Teaching Award, Halliburton Excellent Teaching Award (twice), and Mechanical Engineering Outstanding Faculty Award for Excellence in Teaching and Research (twice). He was recently awarded the Golden Torch Faculty Award for Outstanding Scholarship, Leadership, and Service by the Oklahoma State University/National Mortar Board Honor Society. Dr. Ghajar is a Fellow of the American Society of Mechanical Engineers (ASME) and the Editor-in-Chief of *Heat Transfer Engineering*.

Lap Mou Tam is an Associate Professor and Department Head of Electromechanical Engineering at the University of Macau, Macau, China. He received his Ph.D. in 1995 from Oklahoma State University. His research interests include single and multiphase heat transfer, indoor air quality, and energy saving.

Sik Chung Tam is an Associate Professor of Mathematics at the University of Macau, Macau, China. He received his Ph.D. in 1993 from the University of Missouri-Columbia. His main research interests are the quasi-Banach space theory, statistical learning theory, and the applications of computational intelligence. He is currently developing a neural system for predicting Macau's air quality.